Fluid and registered phases in the second layer of ^{3}He on graphite

M. C. Gordillo

Departamento de Sistemas Físicos, Químicos y Naturales, Universidad Pablo de Olavide, E-41013 Seville, Spain

J. Boronat

Departament de Física, Universitat Politècnica de Catalunya, Campus Nord B4-B5, E-08034 Barcelona, Spain

A quantum Monte Carlo approach, considering all the corrugation effects, was used to calculate the complete phase diagram of the second ^{3}He layer adsorbed on graphite. We found that a first-layer triangular solid was in equilibrium with a gas in the second layer. At a surface density 0.166 ± 0.001 Å^{-2}, this fluid changes into two first-layer registered phases: 4/7 and 7/12 solids. The 7/12 arrangement transforms into an incommensurate triangular structure of $\rho = 0.189 \pm 0.001$ Å^{-2} upon further helium loading. A recently proposed hexatic phase was found to be unstable with respect to those commensurate solids.

Helium adsorbed on graphite at temperatures close to zero is a standard setup to study the properties of stable quasi-two-dimensional quantum fluids and solids [1]. The interplay between the additional third dimension, the effects of the corrugation of the different substrates, and the quantum statistics of the adsorbed isotope (^{4}He is a boson and ^{3}He a fermion) produce very rich phase diagrams. In particular, there is a wealth of experimental data on the behavior of ^{3}He atoms adsorbed on graphite, both on the first (clean or preplated) and second layers [2–15]. Recent experimental [12,13] and theoretical [16,17] work suggests that the low-temperature phase diagram of the first layer includes a liquid-gas coexistence, followed by a solidification at high ^{3}He densities (first to a $\sqrt{3} \times \sqrt{3}$ registered solid and then to an incommensurate one via another set of commensurate structures), and by second-layer promotion [3]. It is worth noticing that the transition from gas to liquid is rather unique in quantum fluids and can be properly modeled only if the corrugation of the substrate is fully taken into account. Once promoted to the second layer, ^{3}He atoms appear to be in a fluidlike phase, that eventually turns into a solid upon increase in the amount of helium adsorbed [3,6–8,10,11,15].

The theoretical knowledge of that second ^{3}He layer is limited to ^{4}He-preplated graphite [16,18]. A full calculation of that phase diagram [18] produced a set of results that compared favorably with the experimental data, predicting the existence of a very dilute liquid that, at higher densities, is in equilibrium with a registered 7/12 solid that progresses to the formation of an incommensurate triangular phase close to third-layer promotion. The density of that commensurate structure compares very favorably to that found experimentally [6–11,19]. However, some caution has to be exercised in comparing the areal densities in a theoretical calculation (simply the number or atoms divided by the surface) to the same experimental magnitude. Calorimetric measurements are typically given in terms of coverage, i.e., as a certain amount in excess of the density corresponding to the first-layer commensurate $\sqrt{3} \times \sqrt{3}$ solid. This could produce a sizable discrepancy

(up to 8.5% [20]) with its neutron scattering counterparts, and therefore some uncertainties in the comparison to our simulations, further complicated with the presence of defects that vary from one sample to another. On the other hand, those theoretical results also indicate that an accurate description of the phase diagram demands the consideration of both the corrugation of the substrates and the relaxation of the first-layer atoms from their crystallographic positions.

In this Rapid Communication, we will be concerned with the quantum Monte Carlo description of a ^{3}He layer on top of an incommensurate ^{3}He solid adsorbed on graphite. As in Ref. [18], the description of the system will be as realistic as possible, including corrugation and relaxation effects. In addition, we also analyzed different first-layer densities to allow for a compression upon helium loading. A recent suggestion [15] about the observation of a stable hexatic ^{3}He phase will be also considered.

The starting point of our microscopic approach is the Hamiltonian for a system with two ^{3}He layers adsorbed on graphite,

$$H = -\frac{\hbar^2}{2m} \sum_{i=1}^{N} \nabla_i^2 + \sum_{i=1}^{N} V_{\text{ext}}(\mathbf{r}_i) + \sum_{i<j}^{N} V(r_{ij}), \quad (1)$$

where m is the ^{3}He mass, and N represents the total number of atoms (on both first and second layers) at positions $\mathbf{r}_i$. The second term in Eq. (1) corresponds to the sum of all individual C-He interactions, modeled by the accurate Carlos and Cole interatomic potential [21]. The graphite sheets containing the carbon atoms were simulated in the same way as in previous literature [17,18,22–25]. $V(r_{ij})$ stands for the helium-helium Aziz potential [26], a standard of the theoretical descriptions of helium at low temperatures. Here, r_{ij} is the distance between any two helium atoms, irrespective of their location on the first or second layer.

We solved the many-body Schrödinger equation associated to the Hamiltonian of Eq. (1) by using the fixed-node diffusion Monte Carlo (FN-DMC) method [27]. This technique provides

us with an approximation to the ground state of the system, a ground state that is expected to be a good description of the real experimental setup at the millikelvin temperatures characteristic of these studies. The sign problem of a Fermi system, like a set of ^{3}He atoms, prevents an exact calculation, in opposition to what happens for bosonic ^{4}He. However, the fixed-node approximation is a stable technique that furnishes us with an upper bound for the ground-state energy of a system of fermions. In the FN-DMC method, the nodes of the ground-state wave function are imposed to be the same as those of a trial wave function (initial approximation to the real wave function). Unfortunately, the position of the real nodes is unknown *a priori*, but the use of an accurate trial function could leave that upper bound very close to the real value. We used

$$
\Phi(\mathbf{r}_1, \mathbf{r}_2, \ldots, \mathbf{r}_N)
$$
$$
= \Psi_u(\mathbf{r}_1, \mathbf{r}_2, \ldots, \mathbf{r}_{N_u}) \Psi_d(\mathbf{r}_{N_u+1}, \mathbf{r}_{N_u+2}, \ldots, \mathbf{r}_N), \quad (2)
$$

with $\mathbf{r}_1, \mathbf{r}_2, \ldots, \mathbf{r}_{N_d}$ the coordinates of the N_u helium atoms on the second layer, and $\mathbf{r}_{N_u+1}, \mathbf{r}_{N_u+2}, \ldots, \mathbf{r}_N$ the ones for the $N_d = N - N_u$ atoms in direct contact with graphite. Following Ref. [18], we considered as the trial wave function for the upper layer

$$
\Psi_u(\mathbf{r}_1, \mathbf{r}_2, \ldots, \mathbf{r}_{N_u}) = D^{\uparrow} D^{\downarrow} \prod_i^{N_u} u_u(\mathbf{r}_i) \prod_{i<j}^{N_u} \exp\left[-\frac{1}{2}\left(\frac{b}{r_{ij}}\right)^5\right],
$$
$$(3)$$

with $D^{\uparrow}$ and $D^{\downarrow}$ the two-dimensional Slater determinants for spin-up and -down atoms, respectively. The coordinates of the particles included in those determinants were corrected by backflow terms in the standard way,

$$
\tilde{x}_i = x_i + \lambda \sum_{j \neq i} \exp[-(r_{ij} - r_b)^2/\omega^2](x_i - x_j), \quad (4)
$$

$$
\tilde{y}_i = y_i + \lambda \sum_{j \neq i} \exp[-(r_{ij} - r_b)^2/\omega^2](y_i - y_j). \quad (5)
$$

Here, $\lambda = 0.35$; $\omega = 1.38$ Å, and $r_b = 1.89$ Å [17,28]. We considered unpolarized systems, i.e., $N_d = N_u = N/2$. The function $u_u(\mathbf{r})$ is the numerical solution of the one-body Schrödinger equation that describes a single ^{3}He atom on top of a triangular lattice formed by first-layer ^{3}He atoms located in the crystallographic positions of an incommensurate triangular phase, neglecting the influence of the graphite structure [17]. In the present work, we used three first-layer triangular lattices of densities taken from different experimental works: 0.109 (from Ref. [3]), 0.113 (intermediate from those of Refs. [20,29]), and 0.116 Å^{-2} (from Ref. [15]). This was done in order to take into account a possible compression of the bottom layer upon increasing the overall helium density. The value of b was optimized variationally ($b = 2.96$ Å).

The bottom-layer trial wave function was

$$
\Psi_d(\mathbf{r}_{N_u+1}, \mathbf{r}_{N_u+2}, \ldots, \mathbf{r}_N)
$$
$$
= \prod_i^{N_d} u_d(\mathbf{r}_i) \prod_{i<j}^{N_d} \exp\left[-\frac{1}{2}\left(\frac{b}{r_{ij}}\right)^5\right]
$$
$$
\times \prod_i^{N_d} \exp\{-a[(x_i - x_{\text{site}})^2 + (y_i - y_{\text{site}})^2]\}. \quad (6)
$$

The last (Nosanov) term compels the atoms to stay close around their crystallographic positions $\{x_{\text{site}}, y_{\text{site}}\}$. $u_d(\mathbf{r}_i)$ is the numerical solution of the one-body Schrödinger equation for one ^{3}He atom on top of graphite, and a was set to 0.24 Å^{-2} as in previous work [17]. The solid phases of the upper layer were also simulated by multiplying Eq. (3) by a Nosanov term, as in Eq. (6).

The possible existence of an hexatic phase in the second layer was also studied by multiplying Eq. (3) by [30]

$$
\psi_h = \prod_{i<j}^{N_u} \exp\left[\alpha \frac{\cos(m\phi_{ij}) - 1}{r_{ij}}\right], \quad (7)
$$

with $\cos(\phi_{ij}) = \frac{\mathbf{r_j} - \mathbf{r_i}}{r_{ij}}$. The value of the variational constants m and α was taken from Ref. [30].

We followed here the methodology used previously to describe two ^{4}He layers adsorbed on graphene [31]. Thus, we started by considering different first-layer triangular lattice densities and calculated the energies for the entire set of atoms (irrespectively of their location on the first or second layer). The first set of data, corresponding to low second-layer densities, is displayed in Fig. 1. In order to obtain the stability ranges of the different phases, we performed double-tangent Maxwell constructions using our FN-DMC results. This means that the x axis in Fig. 1 represents the inverse of the total (first + second layer) density. In that figure, full squares were taken from Ref. [17] and correspond to the incommensurate solid phase of the (single) first layer. Full circles stand by the results from a simulation including 16×9 triangular lattice cells (52.08×50.74 Å^2; 288 ^{3}He atoms) in the first layer plus the necessary atoms in the second one to account for the displayed surface per atom. This corresponds to a bottom layer of density $\rho = 0.109$ Å^{-2}, in line with experimental results of Ref. [3]. Open squares are simulation data for a first layer comprising 14×8 similar cells to give us a bottom-layer density of 0.113 Å^{-2} (44.8×44.34 Å^2; 224 atoms). It can be seen that the open squares are consistently above the open circles in the inverse density range displayed. Therefore, we should draw the double-tangent Maxwell line (dashed line in Fig. 1) between the 0.109 Å^{-2} data and the results for a single-layer solid. From that line, we can establish that a single-layer structure of density 0.106 ± 0.002 Å^{-2} is in equilibrium with a two-layer system with total density 0.111 ± 0.002 Å^{-2}. This means that from 0.106 Å^{-2} up, one would have a mixture of clean first-layer zones with very dilute second-layer systems of $0.111 - 0.109 = 0.002$ Å^{-2} in adequate proportions to produce total intermediate densities
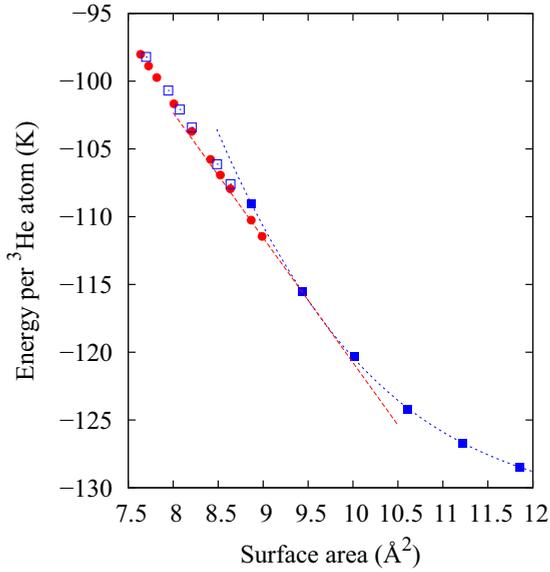
FIG. 1. Energy per ^{3}He atom as a function of the inverse of the total ^{3}He density. Full squares: a single-layer incommensurate solid; full circles:, a second- layer system including a first-layer solid of density 0.109 Å^{-2}; open squares: second-layer arrangement on top of a 0.113 Å^{-2} incommensurate triangular phase. Dotted line: third-order polynomial fit to the single-layer energy values, intended as a guide to the eye; dashed line: double-tangent Maxwell line to determine the coexistence between phases.

in the range from 0.106 to 0.111 Å^{-2}. This is in excellent agreement with the experimental values given in Refs. [2] ($\sim$0.108 Å^{-2}), [8] ($\sim$0.106 Å^{-2}), and [20] ($\sim$0.105 Å^{-2}), obtained with different techniques.

The energy when we increase the density (or decrease the surface per atom), is displayed in Fig. 2. The symbols are the same as in Fig. 1, but we included a third set of calculations (open circles) in which the underlying incommensurate solid density was 0.116 Å^{-2}, following the experimental findings of Ref. [15]. Two things are immediately apparent: first, this last setup is always metastable with respect to the first two arrangements, and second, on increasing the helium density, the energies corresponding to the open squares start to go below the ones represented by full circles. This means that the first-layer solid undergoes a compression upon helium loading. This is in line with previous results for a double ^{4}He layer on graphene. Third-order polynomial fits to the data in Fig. 2, not shown for simplicity, indicate that the crossing is produced at a density $\rho = 0.156 \pm 0.002$ Å^{-2} (6.41 ± 0.01 Å^2 in Fig. 2). This corresponds to a second-layer density of 0.045 ± 0.002 Å^{-2}.

Figure 3 reports the coexistence between the second-layer fluid (open squares), and the 4/7 and 7/12 registered structures with the first layer (full triangles). The dotted line is a double-tangent Maxwell line between the 4/7 solid and a fluid of density 0.166 ± 0.001 Å^{-2} (6.01 ± 0.01 Å^2 in Fig. 3). In both cases, the underlying first-layer density was 0.113 Å^{-2}, since a more compressed triangular solid increases the overall energy per particle. This result is in good agreement
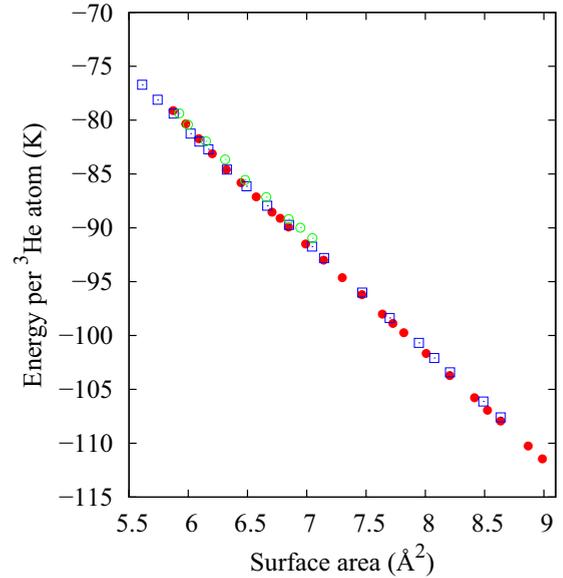

FIG. 2. Energy per ^{3}He atom for three second-layer arrangements, with different densities of the underlying first-layer solid, as a function of the inverse of the total density. Full circles: $\rho = 0.109$ Å^{-2}; open squares: $\rho = 0.113$ Å^{-2}; open circles: $\rho = 0.116$ Å^{-2}.

with the experimental 0.111 Å^{-2} value provided in Ref. [20]. Since the line can be prolonged to higher densities to include the 7/12 structure, we conclude that our results support the coexistence between *both* registered solids and the 0.166 Å^{-2} fluid. This is not surprising given their very close densities ($\rho_{4/7} = 0.177$ Å^{-2}, $\rho_{7/12} = 0.179$ Å^{-2}). In the same figure,
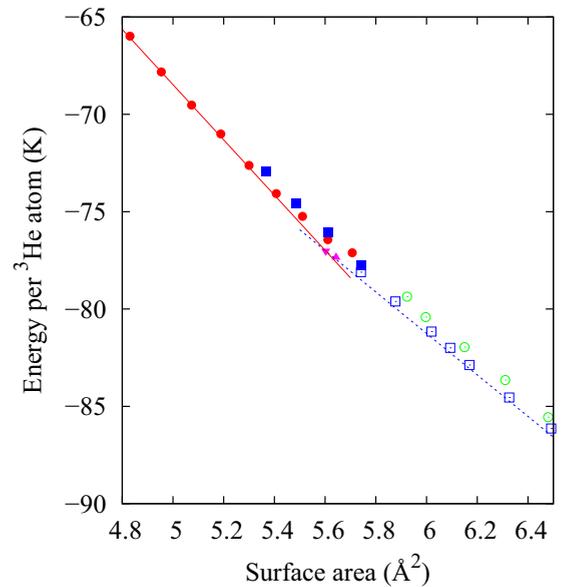

FIG. 3. Same as in the previous figure, but including a double-layer incommensurate solid (upper full circles), an hexatic phase (full squares), and a 4/7 (up triangle) and a 7/12 (down triangle) commensurate phase on top of a first-layer solid of density 0.113 Å^{-2}. Full and dotted lines correspond to Maxwell constructions between the different stable phases.
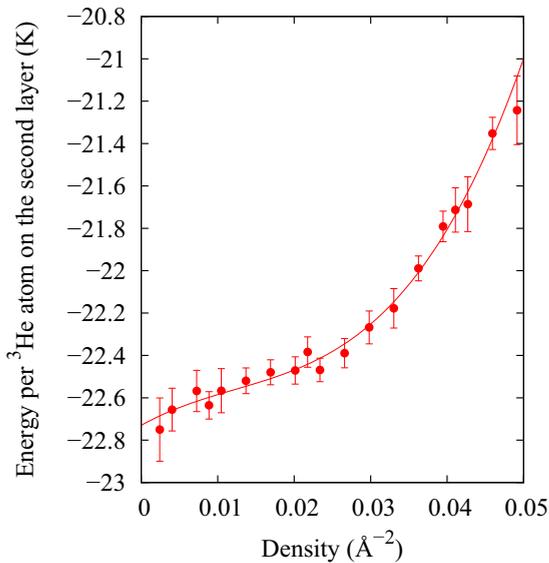
FIG. 4. Energy per ^{3}He atom on the second layer as a function of that layer density. The density of the first layer was $\rho = 0.109$ Å^{-2}. Full line: third-order polynomial fit to the simulation data, intended exclusively as a guide to the eye.

full circles stand for the energy results for the hexatic phase recently proposed in Ref. [15] to account for the experimental data. As we can see, those data are above both the results of the commensurate structures, and the second-layer incommensurate triangular solid represented by the full circles. This means that this phase is unstable with respect to any of those solids, at least in the limit $T = 0$.

The full line in Fig. 3 is another double-tangent Maxwell line, this time between the 7/12 structure and a second-layer incommensurate solid of $\rho = 0.189 \pm 0.001$ Å^{-2} (5.30 ± 0.01 Å^2 in Fig. 3). This density is rather close to the one corresponding to the third-layer promotion observed in different experiments ($\rho = 0.184$ Å^{-2} Ref. [3]; $\rho = 0.186$ Å^{-2}, Ref. [7]; $\rho = 0.187$ Å^{-2}, Ref. [32]; $\rho = 0.19$ Å^{-2}, Ref. [11]). Those values are smaller or compatible with the ones deduced from our data in Fig. 3. This implies that experimentally we should have an equilibrium between a clean second-layer 7/12 structure of $\rho = 0.179$ Å^{-2} and a setup with a low-density fluid on top of a second-layer solid [3,7,11]. The nature of the

transformations undergone by the second layer upon further helium loading is beyond the scope of the present work.

At this point, a remaining question is that of the nature of the second-layer fluid before solidification. To solve that, we plotted the energies per ^{3}He atom *on the second layer* versus the ^{3}He density on that layer alone. This is done in Fig. 4. As one can see, our FN-DMC results correspond to a gas phase, since the energy per atom increases monotonically as a function of the ^{3}He density, with no discernible plateau that would be the telltale signal of a liquid-gas transition [17].

In summary, we have undertaken the calculation of the rather complicated equation of state of the second layer of ^{3}He on graphite. The comparison between previous theoretical descriptions of the same system on preplated graphite [16,17] and the experimental data suggested the necessity of including in the calculations all corrugation and dynamic effects. That implies the consideration of different first-layer densities to take into account a possible compression, in line with what happened for ^{4}He on graphene. With all that, our quantum Monte Carlo results compare very favorably with the available experimental data. This is true for the second-layer promotion density $\rho = 0.106$ Å^{-2} [8] and the upper density limit for a fluid (0.053 Å^{-2} versus the 0.055 Å^{-2} of Ref. [3], and the 0.050–0.060 Å^{-2} interval proposed in Ref. [6]). The solidification into the registered structures is also well predicted ($\rho \sim 0.178$ Å^{-2}, the same value as experiments [7,11]). This also validates our value for the first-layer density upon compression (0.113 Å^{-2}), and differs from the one proposed in Ref. [15] (0.116 Å^{-2}).

Our data also suggest that the registered 4/7 and 7/12 solids are in equilibrium with a three-layer system of $\rho \sim 0.19$ Å^{-2}. This means that from $\rho = 0.179$ Å^{-2} up there is a mixture of second-layer 4/7 and 7/12 structures and a third-layer fluid. Again this agrees with previous experimental findings [10,11], but not with the suggestion of a stable hexatic phase around the same density range. This means that the suggested hexatic phase can hardly be a candidate for the quantum spin liquid proposed in Ref. [15].

[1] L. W. Bruch M. W. Cole, and E. Zaremba, *Physical Adsorption: Forces and Phenomena* (Oxford University Press, Oxford, 1997).

[2] S. W. Van Sciver and O. E. Vilches, Phys. Rev. B **18**, 285 (1978).

[3] D. S. Greywall, Phys. Rev. B **41**, 1842 (1990).

[4] D. S. Greywall and P. A. Busch, Phys. Rev. Lett. **65**, 64 (1990).

[5] H. Godfrin, R. E. Rapp, K. D. Morhard, J. Bossy, and C. Bauerle, Phys. Rev. B **49**, 12377 (1994).

[6] K. D. Morhard, C. Baüerle, J. Bossy, Y. Bunkov, S. N. Fisher, and H. Godfrin, Phys. Rev. B **53**, 2658 (1996).

[7] M. Siqueira, J. Nyeki, B. Cowan, and J. Saunders, Phys. Rev. Lett. **76**, 1884 (1996).

[8] C. Bäuerle, Y. Bunkov, A. S. Chen, S. N. Fisher, and H. Godfrin, J. Low Temp. Phys. **110**, 333 (1998).

[9] M. Roger, C. Bauerle, H. Godfrin, L. Pricoupenko, and J. Treiner, J. Low Temp. Phys. **112**, 451 (1998).

[10] E. Collin, S. Triqueneaux, R. Harakaly, M. Roger, C. Bäuerle, Y. M. Bunkov, and H. Godfrin, Phys. Rev. Lett. **86**, 2447 (2001).

[11] H. Fukuyama, J. Phys. Soc. Jpn. **77**, 111013 (2008).

[12] D. Sato, T. Tsuji, S. Takayoshi, K. Obata, T. Matsui, and H. Fukuyama, J. Low Temp. Phys. **158**, 201 (2010).

[13] D. Sato, K. Naruse, T. Matsui, and H. Fukuyama, Phys. Rev. Lett. **109**, 235306 (2012).

[14] Ashley G. Smart, Phys. Today **66** (1), 16 (2013).

[15] S. Nakamura, K. Matsui, T. Matsui, and H. Fukuyama, Phys. Rev. B **94**, 180501(R) (2016).

[16] M. Ruggeri, E. Vitali, D. E. Galli, M. Boninsegni, and S. Moroni, Phys. Rev. B **93**, 104102 (2016).

[17] M. C. Gordillo and J. Boronat, Phys. Rev. Lett. **116**, 145301 (2016).

[18] M. C. Gordillo and J. Boronat, Phys. Rev. B **94**, 165421 (2016).

[19] C. Bäuerle, Y. M. Bunkov, S. N. Fisher, and H. Godfrin, Czech. J. Phys. **46** S1 401 (1996).

[20] H. Godfrin and H. J. Lauter, Experimental properties of ^{3}He adsorbed on grephite, in *Progress in Low Temperature Physics*, Vol. XIV, edited by W. P. Halperin (Elsevier Science B.V., Amsterdam, 1995), p. 213.

[21] W. E. Carlos and M. W. Cole, Surf. Sci. **91**, 339 (1980).

[22] M. C. Gordillo and J. Boronat, Phys. Rev. Lett. **102**, 085303 (2009).

[23] M. C. Gordillo, Phys. Rev. B **89**, 155401 (2014).

[24] M. C. Gordillo, C. Cazorla, and J. Boronat, Phys. Rev. B **83**, 121406(R) (2011).

[25] M. C. Gordillo and J. Boronat, J. Low Temp. Phys. **171**, 606 (2013).

[26] R. A. Aziz, F. R. W McCourt, and C. C. K. Wong, Mol. Phys. **61**, 1487 (1987).

[27] B. L. Hammond, W. A. Lester, Jr., and P. J. Reynolds, *Monte Carlo Methods in Ab Initio Quantum Chemistry* (World Scientific, Singapore, 1994).

[28] J. Casulleras and J. Boronat, Phys. Rev. Lett. **84**, 3121 (2000).

[29] F. Ziouzia, J. Nyeki, B. P. Cowan, and J. Saunders, J. Low Temp. Phys. **134**, 85 (2004).

[30] V. Apaja and M. Saarela, Europhys. Lett. **84**, 40003 (2008).

[31] M. C. Gordillo and J. Boronat, Phys. Rev. B **85**, 195457 (2012).

[32] M. Siqueira, Jan Nyeki, B. Cowan, and J. Saunders, Phys. Rev. Lett. **78**, 2600 (1997).